Available online at www.sciencedirect.com
ScienceDirect
European Journal of Mechanics B/Fluids 25 (2006) 971–986

Experiments on the linear instability of flow in a wavy channel

M. Asai [a], J.M. Floryan [b,*]

[a] *Department of Aerospace Engineering, Tokyo Metropolitan University, Asahigaoka 6-6, Hino, Tokyo 191-0065, Japan*
[b] *Department of Mechanical and Materials Engineering, The University of Western Ontario, London, Ontario, Canada, N6A 5B9*

Received 7 October 2005; received in revised form 8 February 2006; accepted 21 March 2006

Available online 6 May 2006

Abstract

The effects of wall corrugation on the stability of wall-bounded shear flows have been examined experimentally in plane channel flows. One of the channel walls has been modified by introduction of the wavy wall model with the amplitude of 4% of the channel half height and the wave number of 1.02. The experiment is focused on the two-dimensional travelling wave instability and the results are compared with the theory [J.M. Floryan, Two-dimensional instability of flow in a rough channel, Phys. Fluids 17 (2005) 044101 (also: Rept. ESFD-1/2003, Dept. of Mechanical and Materials Engineering, The University of Western Ontario, London, Ontario, Canada, 2003)]. It is shown that the flow is destabilized by the wall corrugation at subcritical Reynolds numbers below 5772, as predicted by the theory. For the present corrugation geometry, the critical Reynolds number is decreased down to about 4000. The spatial growth rates, the disturbance wave numbers and the distribution of disturbance amplitude measured over such wavy wall also agree well with the theoretical results.

Keywords: Laminar-turbulent transition; Roughness effects; Plane channel flow

1. Introduction

Understanding how surface roughness affects the laminar-turbulent transition process in shear layers is one of the fundamental questions in fluid dynamics. This question is of practical interest in several applications areas, i.e., laminar airfoils, compact heat exchangers, laminar electrostatic precipitators, atmospheric boundary layers, etc. Flows over rough walls have been studied since the early works of Hagen [2] and Darcy [3] focused on turbulent flows, however, Reynolds [4] was the first to pose the problem in the context of laminar-turbulent transition. In spite of many attempts [5] the resolution of this problem is still uncertain.

The original experimental investigations were focused on flows in circular pipes and the various possible roughness forms were classified using the concept of "equivalent roughness"; see Jimenez [6] for a recent review. The phenomenological effects of the "equivalent roughness" are summarized in the form of friction coefficient [7–9]. These and other similar investigations show that surface roughness contributes directly to the dynamics of flow only if the wall is hydraulically rough. Precise definition of the hydraulic smoothness is, however, not available. While the modelling concepts of this type have been being continuously re-evaluated [10] and improved [11], they failed so far to uncover

* Corresponding author.
E-mail address: mfloryan@eng.uwo.ca (J.M. Floryan).

0997-7546/$ – see front matter
doi:10.1016/j.euromechflu.2006.03.002

the mechanisms that govern the complex, flow-condition-dependent interaction between the roughness geometry and the moving fluid.

The existing experimental evidence dealing with the laminar-turbulent transition shows that mechanisms activated by the roughness depend on the surface geometry [1]. The possible geometries can be conveniently divided into three classes, i.e., isolated two-dimensional roughness, isolated three-dimensional roughness and distributed roughness. The first case corresponds to spanwise trip wire where the onset of transition is believed to be associated with the instability of inflectional separated velocity profiles [12,13]. In the second case, downstream legs of horseshoe vortices generate strong inflectional shear layers whose instabilities are believed to be responsible for the onset of transition [14], similarly as in the case of Görtler instability [15]. In the third case, the presence of distributed roughness leads to an explosive departure from the laminar state [16], however, the mechanics of this process is not understood. The present investigation is focused on the identification of the mechanisms associated with distributed roughness.

Presence of distributed roughness distorts the average velocity profile, but analysis of stability of such profiles proved inconclusive [17–19]. Concepts based on the roughness-induced additional mixing were not successful either [20]. Attempts to explain roughness effects in terms of Tollmien–Schlichting waves [14,21] were inconclusive. Floryan [22] proposed a completely different approach, where the problem is split into two steps, i.e., the basic state that accounts for the spatial structure of the roughness is determined first and is followed by the stability analysis that must account for the spatial structure of the roughness beyond a simple change of the average velocity profile. The geometry of the roughness is represented in terms of Fourier expansions, which reduces the analysis of the effects of different geometries to scans of parameter space formed by the coefficients of the expansions. Wavy wall geometry is represented in terms of a single Fourier mode and thus forms the simplest and most convenient reference case. Brevdo and Bridges [23] provide a general discussion of stability of spatially periodic systems.

Two classes of unstable disturbances have been identified in the case of wavy wall geometries. The first one involves streamwise vortices, which are induced when critical conditions are met [24,25]. These conditions involve a correct combination of the corrugation amplitude, the corrugation wave number and the flow Reynolds number. If the corrugation amplitude is smaller than a certain critical value, the vortices will not be destabilized regardless of the value of the Reynolds number. Similarly, if the corrugation wave number falls outside a certain well defined range, the vortices will not appear. The strength of the instability rapidly increases with the corrugation amplitude and the flow Reynolds number. The second mode of instability involves travelling waves whose dynamics in the case of flow in a wavy channel has been discussed by Floryan [1]. Increase of the corrugation amplitude decreases the critical Reynolds number, with the corrugation wave number O(10) being most effective. Again, the strength of the instability rapidly increases with the corrugation amplitude.

The non-linear effects that drive the transition process may be induced through a transient growth without involving any linear instability [26]. The transient growth is a linear process that relies on the non-orthogonality between modes resulting in a growth of disturbance energy even when all modes decay. This process always occurs in shear layers, but is relevant in the case of noisy environment where the initial disturbance amplitudes are large enough so that transient growth can reach the level necessary to trigger non-linear effects. One needs to note that the amplitudes and phases of disturbances need to be adjusted properly in order to produce significant transient effect. While surface roughness may amplify this process [27], its role remains to be substantiated.

The present work is focused on the experimental verification of the theory describing travelling wave instability in a channel with wavy wall [1]. It is known that the travelling wave instability in a smooth channel occurs for $Re > 5772$ and that the critical disturbance has the form of two-dimensional wave travelling in the streamwise direction. Theoretical description of this instability involves the celebrated Orr–Sommerfeld (OS) equation [28,29] and the experimental proof has been provided by Nishioka et al. [30]. The OS equation represents a special case of the more general equations applicable in the case of corrugated walls [1,22]. We wish to establish if these equations are able to describe the travelling wave instability process in the presence of wall corrugations. We have selected for the experiment corrugation in the form of wavy wall because this geometry is well defined as well as it represents the first Fourier mode used in the theoretical description of an arbitrary corrugation. Simplicity of this shape and thus ability to carry out well defined and well controlled experiment, as well as ability of wavy wall to approximate properties of more complex geometries [1], provide additional support for this choice.

The manuscript is organized as follows. Section 2 provides a short summary of the theory re-arranged to a form more suitable for experimental verification, i.e., spatial stability theory. Section 3 provides description of the experiment. In particular, Section 3.1 discusses experimental facility, Section 3.2 provides description of the measurements

and verification of the creation of the fully developed Poiseuille flow, Section 3.3 discusses linear instability of the flow in a smooth channel, Section 3.4 provides description of the flow in a channel with a wavy wall, and Section 3.5 discusses linear instability of this flow. A short summary of the main conclusions is given in Section 4.

2. Theory

We shall consider linear, two-dimensional instability of flow in a channel bounded by one flat and one corrugated wall. The corrugation has sinusoidal form characterized by the amplitude S and the wave number α. The theory that describes the effect of the corrugation on the temporal flow stability is been explained in [1]. The spatial formulation more suitable for comparisons with experiments is presented below.

2.1. Basic state

We consider steady, two-dimensional flow in a channel with smooth lower wall and corrugated upper wall. The flow field is represented in the form

$$\begin{aligned} &\boldsymbol{V}_2(x,y) = \big[u_2(x,y), v_2(x,y)\big] = \big[u_0(y), 0\big] + \big[u_1(x,y), v_1(x,y)\big], \\ &p_2(x,y) = p_0(x) + p_1(x,y) = -2x/Re + p_1(x,y), \end{aligned} \tag{2.1}$$

where $u_0 = 1 - y^2$, p_0 describe the reference plane Poiseuille flow and u_1, v_1, p_1 describe modifications associated with the presence of the corrugation. The channel extends from $-\infty$ to $+\infty$ in the x-direction and the locations of the lower and upper walls, i.e., $y_{\mathrm{L}}(x)$ and $y_{\mathrm{U}}(x)$, are defined as $y_{\mathrm{L}}(x) = -1$, $y_{\mathrm{U}}(x) = 1 + (S\,\mathrm{e}^{\mathrm{i}\alpha x} + CC)$, where CC stand for the complex conjugate, and S and α denote the amplitude and the wave number of the corrugation, respectively. The flow is scaled using the maximum of the x-velocity of the reference Poiseuille flow and the average half-channel height h. The flow modifications can be represented using Fourier expansion in the form $\Psi(x,y) = \sum_{n=-\infty}^{n=+\infty} \Phi^{(n)}(y)\,\mathrm{e}^{\mathrm{i}n\alpha x}$ where Ψ represents the stream function defined in the usual manner, i.e., $u_1 = \partial_y \Psi$, $v_1 = -\partial_x \Psi$, $\Phi^{(n)} = \Phi^{*(-n)}$ and star denotes complex conjugate. The field equations can be reduced to equations for $\Phi^{(n)}$, $n \geqslant 0$, in the form

$$\big[D_n^2 - \mathrm{i}n\alpha\,\mathrm{Re}\big(u_0 D_n - D^2 u_0\big)\big]\Phi^{(n)} - \mathrm{i}\alpha\,\mathrm{Re}\sum_{k=-\infty}^{k=+\infty}\big[kD\Phi^{(n-k)}D_k\Phi^{(k)} - (n-k)\Phi^{(n-k)}D_k D\Phi^{(k)}\big] = 0, \tag{2.2}$$

where $D = \mathrm{d}/\mathrm{d}y$ and $D_n = D^2 - n^2\alpha^2$. The boundary conditions that correspond to the fixed mass constraint [22] have the form

$$D\Phi^{(n)} = \Phi^{(n)} = 0 \quad \text{at } y = -1 \quad \text{and} \quad y = y_{\mathrm{U}}, \quad \infty \geqslant n \geqslant 0, \tag{2.3}$$

and can be implemented directly at the lower wall while the immersed boundary conditions concept needs to be used at the upper wall. Problem (2.2), (2.3) has been solved using spectral discretization of $\Phi^{(n)}$ based on the Chebyshev polynomials [1,31].

2.2. Linear stability

Unsteady, two-dimensional disturbances are superimposed on the basic state described previously, resulting in the total stream function expressed as

$$\psi = \psi_2(x,y) + \psi_3(x,y,z,t), \tag{2.4}$$

where subscripts 2 and 3 refer to the basic state and the disturbance field, respectively. Eq. (2.4) is substituted into the field equations, the mean part is subtracted, the equations are linearized and the disturbance stream function is taken in the form

$$\psi_3(x,y,t) = \sum_{m=-\infty}^{m=+\infty} \varphi^{(m)}(y)\,\mathrm{e}^{\mathrm{i}[(\delta+m\alpha)x - \sigma t]} + CC. \tag{2.5}$$

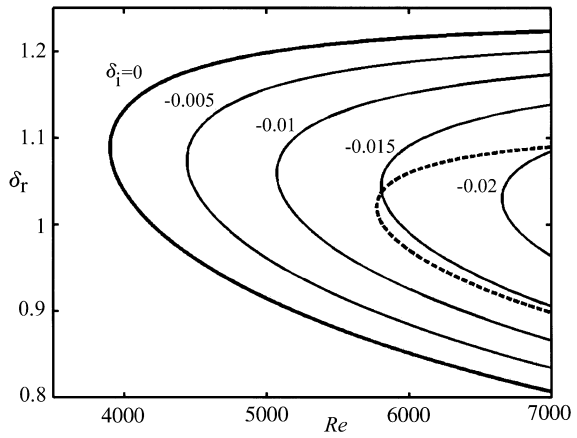

Fig. 1. Linear stability diagram for the spatial instability of the flow in a channel with one wavy wall with the amplitude $S = 0.02$ and the wave number $\alpha = 1.02$. Dash line gives the neutral stability curve for the smooth channel. δ_i and δ_r denote the disturbance amplification rate and the wave number, respectively.

Floryan [1] considered δ real and σ complex, which lead to the temporal stability theory with the imaginary part of σ describing the growth rate. We shall assume in the present analysis that $\delta = \delta_r + i\delta_i$ is complex and σ is real, leading to the spatial stability theory with the disturbance growth rate, wave number and frequency given by δ_i, δ_r and σ, respectively. Separation of Fourier modes leads to a system of equations for $\varphi^{(m)}$, $-\infty < m < +\infty$, in the form

$$S^{(m)}\varphi^{(m)} = i\alpha\,\mathrm{Re}\sum_{n=-\infty}^{n=+\infty}\left[\varepsilon_n D\Phi^{(m-n)}H^{(n)}\varphi^{(n)} + \alpha(m-n)G^{(m-n)}\Phi^{(m-n)}D\varphi^{(n)} - \alpha(m-n)\Phi^{(m-n)}H^{(n)}D\varphi^{(n)} - \varepsilon_n G^{(m-n)}D\Phi^{(m-n)}\varphi^{(n)}\right] \tag{2.6}$$

where $S^{(m)} = (D^2 - \varepsilon_m^2)^2 + i\,\mathrm{Re}(\sigma - \varepsilon_m D\Psi_0)(D^2 - \varepsilon_m^2) + i\,\mathrm{Re}\,\varepsilon_m D^3\Psi_0$ stands for the Orr–Sommerfeld operator and $G^{(n)} = D^2 - n^2\alpha^2$, $H^{(n)} = D^2 - \varepsilon_n^2$, $\varepsilon_n = \delta + n\alpha$, $D = \mathrm{d}/\mathrm{d}y$, $\Psi_0 = -y^3/3 + y + 2/3$. We shall consider only disturbances subject to the fixed mass constraint. The relevant boundary conditions [1] have the form

$$\varphi^{(m)} = D\varphi^{(m)} = 0 \quad \text{at } y = -1 \quad \text{and} \quad y = y_U, \quad -\infty < m < +\infty. \tag{2.7}$$

Conditions at the lower wall can be implemented directly, while conditions at the upper wall require use of the immersed boundary conditions concept. Eqs. (2.6) with boundary conditions (2.7) have non-trivial solutions only for certain combinations of parameters δ, σ and α. The required dispersion relation has to be determined numerically [1]. For the purposes of calculations, the problem is posed as an eigenvalue problem for δ.

Fig. 1 displays stability diagram for the wavy wall with the amplitude $S = 0.02$ and the wave number $\alpha = 1.02$. The critical conditions for the onset of the instability are $Re_{cr} = 3900$, $\delta_{r,cr} = 1.09$, $\sigma_{cr} = 0.312$. The same figure shows the neutral stability curve in the case of smooth wall. In both cases, the unstable disturbances have the form of travelling waves. It can be seen that the presence of the corrugation is responsible for significant destabilization of the flow.

3. Experiments

The experiment has been designed to verify the theory summarized in the previous section. Controlled disturbances were introduced upstream of the wavy wall model and their growth above the corrugated wall was measured and compared with the theoretical predictions. We shall begin our discussion with the description of the experimental facility, followed by the description of the tests carried out to assure that the basic-state corresponded to that described in Section 2.1, and ends with the description of the results of the measurements of the disturbance growth. The measurements have been carried out initially with a flat wall model to test the flow response to controlled disturbances, and then repeated with the wavy wall model to determine changes in the flow response induced by the corrugation.

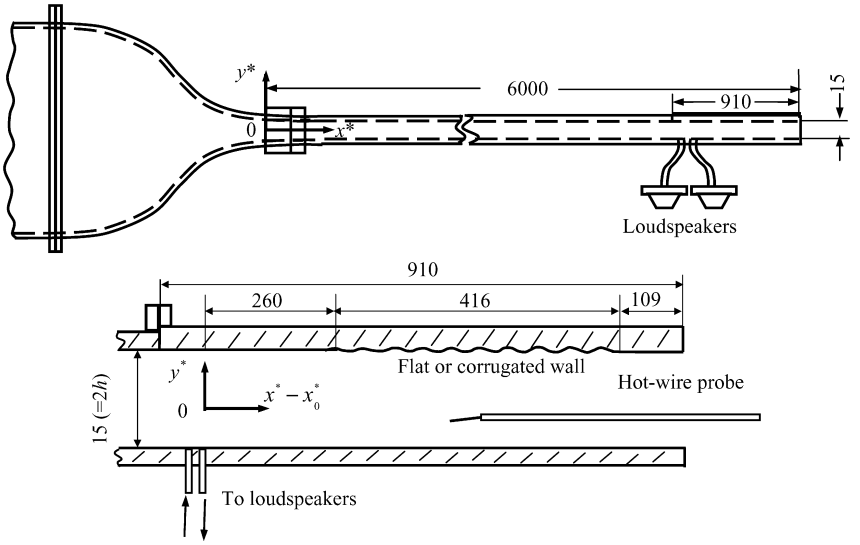

Fig. 2. Schematic diagram of the wind tunnel and the test section (dimensions in mm).

3.1. Experimental set up and procedure

The experiments were conducted in a rectangular wind channel, whose width, height and length were 400 mm, 15 mm (=2h) and 6000 mm, respectively. The schematic diagram of the channel is shown in Fig. 2. The (x, y, z) coordinate system was introduced for reference purposes, with the x, y, z axes overlapping with the streamwise, normal-to-the-wall and spanwise directions, respectively. The origin of the system was placed at the entrance to the channel, with the upper wall corresponding to $y = y^*/h = 1$, the lower wall to $y = y^*/h = -1$, and the sidewalls to $z = z^*/h = \pm 26.7$; the aspect ratio of the channel cross-section was 26.7. Here stars denote dimensional quantities. The channel half-height h used as the reference length scale to define the Reynolds number was 7.5 mm. The channel was built using smooth Plexiglas. Section of the upper wall downstream from $x = x^*/h = 680$ ($x^* = 5100$ mm) could be replaced with a special model in order to investigate the effect of wall waviness. The detail of the wavy wall model will be explained in Section 3.4.

The flow was generated by a fan system at the upstream end of the channel and was discharged to the atmosphere at the downstream end. The maximum streamwise velocity U_c at the channel half-height had been varied from 0 to 12 m/sec, giving the maximum value of Reynolds number $Re = 6000$. The low level of turbulence was achieved through the use of a 1100 mm long settling chamber with 400 × 400 mm cross-section, that contained in sequence a damping screen made of 40 mesh wire gauze, 80 mm long honeycomb with 6 mm openings, and a set of five additional damping screens placed 200 mm apart. This was followed by a two-dimensional, 720 mm long contraction, which produced area contraction of 26.7. The resulting background turbulence at all Reynolds numbers examined was not higher than 0.1% of U_c. The background turbulence consisted mainly of low-frequency components (less than 30 Hz at $Re = 5000$), and fan noise was less than 0.01% of U_c. It was also confirmed that the flow was kept laminar over the whole span without any lateral contamination.

The experiment involved excitations of two-dimensional disturbances through specially prepared slots. Two thin, transverse slots 300 mm long and 3 mm wide had been cut at the bottom wall at locations $x = 693.3$ and 696 ($x^* = 5200$ mm and 5220 mm). The slots were covered with a thin aluminium plate in which many small holes of 0.4 mm diameter were drilled spaced 0.6 mm apart in the streamwise and spanwise directions. The plate was flushed with the surface of the wall. Each slot was connected with a loudspeaker through a specially designed converging vane. Soft rubber seals were used in the junction to eliminate transfer of vibrations to the channel wall. Two loudspeakers were driven at a single frequency by using sine-wave generator through a power amplifier. The input signals to the two loudspeakers had an equal intensity but were 180° out of phase so that the suction and blowing occurring simultaneously at each instant of time cancelled acoustic disturbances. Adjusting the input voltage to the loudspeakers could easily control the amplitude of the excited disturbance.

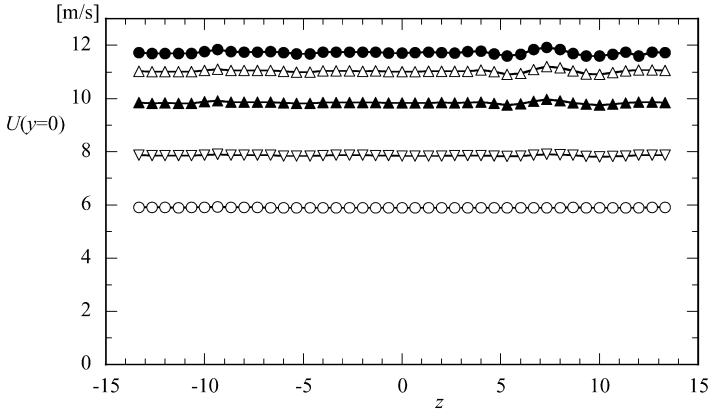

Fig. 3. Spanwise variations of the streamwise velocity at the channel half-height $U(y = 0)$ in the smooth channel at the flow Reynolds numbers $Re = 3000$ (○), 4000 (▽), 5000 (▲), 5600 (△) and 6000 (●). Measurements were made at the channel exit ($x = 800$).

The streamwise velocity component was measured by using a constant temperature hot-wire anemometer. The sensitive length of the hot-wire sensor, a tungsten wire of 5 μm in diameter, was 1 mm. The hot-wire probe was inserted from the downstream end of the channel as shown in Fig. 2. The probe could be traversed in the x, y and z directions. Hot-wire data were stored with the input signal to loudspeakers (reference signal) in a personal computer after 16-bit A/D conversion. In addition, the distributions of the time-mean and the r.m.s. values of the streamwise velocity fluctuations were recorded in an XY plotter during y-traverse. Additional velocity measurements were conducted at the channel exit using a small pitot tube. Static pressure measurements were carried out using pressure holes with 0.4 mm diameter drilled 300 mm apart along the line $z = -13.3$, with the first hole placed at $x = 40$ ($x^* = 300$ mm) to confirm if the flow was fully developed in the test section. A manometer for the pressure measurement had the accuracy of ±0.01 mmAq, which corresponded to ±0.05% of ρU_c^2 at the highest Reynolds number $Re = 6000$.

3.2. Measurements of the basic state in a channel with smooth walls

The stability measurements were made downstream from the slots and thus we shall refer to this part of the channel ($x > 696$) as the test section. It is necessary to ascertain that the base flow in the test section can be regarded as the fully developed, two-dimensional Poiseuille flow.

As a first step, we shall verify the two-dimensional character of the flow. Fig. 3 illustrates spanwise variations of the streamwise velocity component at the channel half height measured at the channel exit for different values of Reynolds number, $Re = 3000$, 4000, 5000, 5600 and 6000. Here the streamwise velocity component of the basic flow is denoted by U in the experiment. It can be seen that the flow was two-dimensional everywhere except region between $5 < z < 14$ where the spanwise variation of the velocity (peak-to-peak value) was at most 2% at $Re = 6000$. In the mid-span region between $-4 < z < 4$, the magnitude of the spanwise variations was less than 0.4% even at $Re = 6000$ and was reduced down to 0.2% at $Re = 5000$. The maintenance of such high two-dimensionality of the flow enabled us to examine the stability characteristics of the flow. We should note that the centre-line velocity averaged over $-4 < z < 4$, denoted by U_c, was used as the reference velocity to define the flow Reynolds number.

As a second step, we shall verify that the flow is fully developed in the test section. Sadri and Floryan [32] have shown theoretically that the flow approaches the fully developed flow exponentially as a function of distance from the channel entry, with the exponent decreasing with an increase of the Reynolds number. The flow in the test section can thus be considered to represent Poiseuille flow only if the test section is sufficiently far away from the channel entry. Before the stability experiment, we examined the flow development in the channel entrance region to confirm if it follows the theory. The streamwise velocity distributions across the channel height and the static pressure distributions in the streamwise direction were carefully measured for $Re = 3000$–6000 [33]. The streamwise variations of the wall pressure that are displayed in Fig. 4 show that the pressure variations (non-dimensionalized with ρU_c^2) upstream of the test section do correspond to those predicted by the theory [32] and approach the linear form ($\mathrm{d}p/\mathrm{d}x = -2/Re$) in the test section. The reader may note that the complete pressure gradient can expressed as $-\mathrm{d}p/\mathrm{d}x = 2/Re + B\,\exp(-\beta x)$

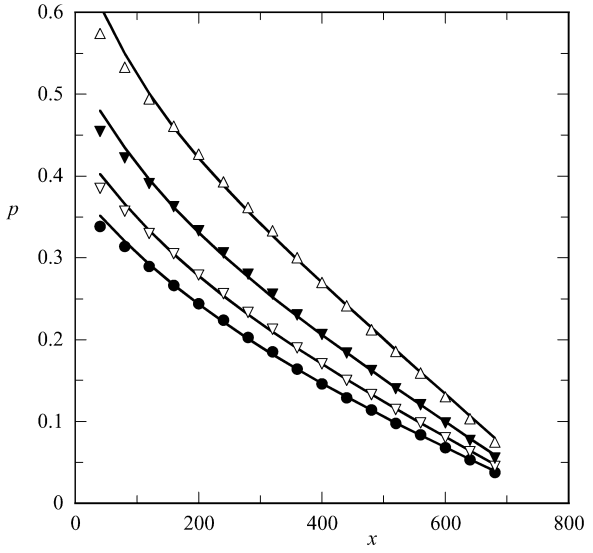

Fig. 4. Pressure distributions in the streamwise (x) direction for the flow Reynolds numbers $Re = 3000$ (△), 4000 (▼), 5000 (▽) and 6000 (●) at $z = 13.3$ in a smooth channel. Solid curves represent theoretical predictions [32], $-\mathrm{d}p/\mathrm{d}x = 2/Re + B\,\exp(-28.221x/Re)$.

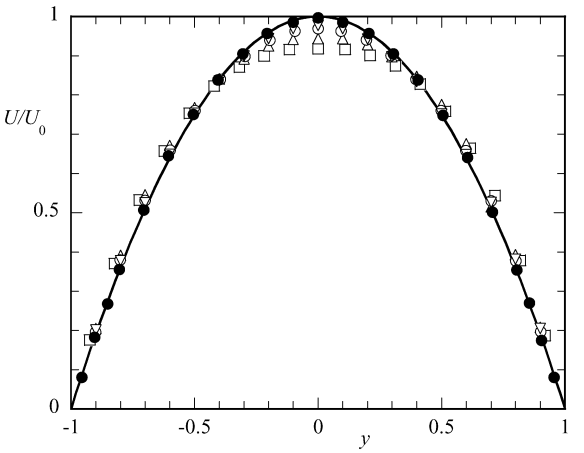

Fig. 5. Profiles of streamwise velocity U measured at $x = 280$ (□), 400 (△), 540 (○), 670 (▽) and 780 (●) at the flow Reynolds number $Re = 6000$ in a smooth channel. The corresponding parabolic profile (solid curve) was obtained in such a way that the flow rate coincided with that of the measured velocity profiles. U_0 is the maximum velocity of the parabolic flow.

with the exponent $\beta = 28.221/Re$ and B representing a constant to be determined from matching with the flow at the channel entry.

Fig. 5 displays y-distributions of the streamwise velocity component $U(y)$ at $x = 280$, 400, 540 670 and 780 for the highest Reynolds number $Re = 6000$ and the corresponding fully develop Poiseuille velocity profile determined in such a way that the flow rates of both flows were the same. Here it should be noted that the calibration error for hot-wire measurement, which was made using a calibration function $U = A(E^2 - B)^{1/n}$ (E is the output voltage of hot-wire anemometer at the velocity U), was at most 0.04 m/sec over the velocity range between 2 m/sec and 12 m/sec, that is, 0.33% of the maximum (line-line) velocity (≈12 m/s) at $Re = 6000$. The deviation of the measured velocity profile from the parabolic profile ΔU decreased downstream. The deviation ΔU at the channel half ($y = 0$) was about 8.1%, 5.7% and 3.0% of the centreline velocity of the developed parabolic flow at $x = 280$, 400 and 540, respectively, which was well correlated with the theoretical prediction, i.e., $\Delta U \propto \exp(-\beta x)$. The deviation ΔU at the middle of the channel ($y = 0$) decreased down to 2% at $x = 670$ and to less than 1% for $x = 780$. Indeed, both the measured and theoretical distributions are practically indistinguishable at $x = 780$. We shall demonstrate in Section 3.3 that such small differences in the velocity distribution have negligible effect on the stability characteristics.

3.3. Linear stability of the flow in a channel with smooth walls

Artificial disturbances were introduced to excite Tollmien–Schlichting (TS) waves using the loudspeaker system described in Section 3.1. It had been observed that the flow disturbance acquired structure that would not change in the streamwise direction at a certain distance downstream from the generator. This distance had been estimated to be no longer than four wavelengths of the TS wave and determined the minimum distance between the test section and the disturbance generator (see Fig. 2).

It is well known that flow in a channel with smooth walls becomes linearly unstable at $Re \approx 5772$ with the critical disturbance having the form of a two-dimensional travelling wave with the dimensionless wave number $\alpha = 1.02$, the frequency $\sigma = 0.2692$, and the streamwise velocity component being anti-symmetric in y. A series of experiments have been carried out in order to demonstrate that the experimental facility can accurately reproduce such instability. In addition, these tests verify that small differences between the actual Poiseuille flow and the flow produced in the test section (e.g., small spanwise variations of the flow, small difference between the fully developed flow and the actual flow) have negligible effect on the measured stability characteristics.

In the absence of corrugation the coupling terms on the right-hand side of (2.14) as well as in the boundary conditions (2.15) are absent and the disturbance equations describe a set of travelling waves independent of each other. The most amplified (or the least damped) eigenmode known as TS wave is observed far downstream of the disturbance generator and its streamwise velocity component $u_3(x, y, t)$ can be written as

$$u_3(x, y, t) = \mathrm{e}^{-\delta_\mathrm{i} x}\left\{u^{(0)}(y)\,\mathrm{e}^{\mathrm{i}(\delta_r x - \sigma t)} + CC\right\}, \tag{3.1}$$

i.e., the disturbance wave propagates along the channel without any modulation while its amplitude grows exponentially with the constant amplification rate δ_i. In order to make comparisons with the experiment, it is convenient to express the disturbance velocity (3.1) as

$$u_3(x, y, t) = \hat{u}_3(y)\,\mathrm{e}^{-\delta_\mathrm{i} x}\cos\left[\delta_\mathrm{r} x - \sigma t - \theta_3(y)\right] \tag{3.2}$$

where $\hat{u}_3(y) = 2|u^{(0)}(y)|$ and $\theta_3(y)$ the phase. The eigenvalue $\delta_\mathrm{r} + \mathrm{i}\delta_\mathrm{i}$ and the eigenfunction $u^{(0)}(y)$ were calculated from the Orr–Sommerfeld equation for a specified frequency σ. In the experiment, on the other hand, $u_3(x, y, t)$is measured at each x-location as

$$u_3(x, y, t) = \sqrt{2}\,u'(x, y)\cos\left[\sigma t + \theta(x, y)\right] \tag{3.3}$$

where $u'(x, y)$ denotes the r.m.s. amplitude and $\theta(x, y)$ the phase. If the disturbance measured consists of the TS mode alone, u_3 takes the form (3.2), with $\theta(x, y) = \theta_3(y) - \delta_\mathrm{r} x$ and $u'(x, y) = \sqrt{2}|u^{(0)}(y)|\,\mathrm{e}^{-\delta_\mathrm{i} x}$. The experiment involved measurements of $u'(x, y)$ and $\theta(x, y)$ to obtain δ_i and δ_r for fixed frequency σ. The disturbance frequency was selected by fixing frequency of the loudspeaker.

Fig. 6 displays theoretical and experimentally measured distributions of the amplitude $u'(y)$ and phase $\theta_0(y)$ for frequency $\sigma = 0.3$ at $Re = 5000$. The measurement was made at $x - x_0 = 53.3$, where x_0 denotes the location of the disturbance generator. The forcing frequency component corresponding to u_3 was extracted from the measured streamwise velocity fluctuations by the Fourier analysis, and θ was obtained relative to the phase of the forcing sine-wave signal. Here the frequency resolution of the Fourier transform was 0.5 Hz. Good agreement between the theory and experiment is noted for both distributions. This agreement is due to the good two-dimensionality of the excited TS wave; this fact is well illustrated in Fig. 7 which displays spanwise distributions of u'_m (the y-maximum of u') and the phase θ measured at $y = -0.85$. Variations (peak to peak values) of u'_m and θ are less than 10% and 15 deg of the average, respectively, for $-10 < z < 8$.

Fig. 8 illustrates streamwise development of disturbances excited with frequency $\sigma = 0.27$ and $\sigma = 0.30$ for $x - x_0 > 20$ at $Re = 4000$, 5000 and 6000. The disturbance development is exponential with constant exponent in all the cases so that slope of each evolution curve determines the growth rate. Besides, the fact that the growth rate is almost constant from $x - x_0 = 20$ ($20h$ downstream of the disturbance generator) strongly suggests that the least damped TS wave has already been dominant for $x - x_0 > 20$. Fig. 9 illustrates the corresponding streamwise variation of disturbance phase $\theta(x, y)$ measured at a fixed y-position ($y = -0.7$) for $\sigma = 0.24$, 0.27, 0.30, 0.33 and 0.36 at $Re = 5000$. If the disturbance behaves as a single TS mode, the phase changes in proportion to $-\delta_\mathrm{r} x$. As expected, the phase $\theta(x, y)$ changes linearly with x, and the slope of each curve provides the wave number δ_r of the disturbance. Fig. 10(a) displays measured growth rates together with those computed on the basis of linear stability theory. The determination of the growth rates from the experimental data was made by the least square method. Good agreement between the theory and experiment is noted. The differences in the measured and theoretical growth rates observed for higher frequencies come from small differences in the wave number–frequency relation that is difficult to establish experimentally for high frequencies. The source of these differences is difficult to identify precisely; similar differences, although bigger in absolute sense, were also reported by Nishioka et al. [30]. Much better agreement is observed when the growth rate is plotted against the wave number. It is important to note that the magnitude of disturbances was at most 0.3% in terms of $u'_\mathrm{m}/U_\mathrm{c}$ in all the cases. Such amplitude is sufficiently smaller than the threshold required (about 0.7% in terms of $u'_\mathrm{m}/U_\mathrm{c}$) to initiate the secondary instability [34] leading to the so-called peak-valley wave growth [35]. Fig. 10(b) illustrates variations of the disturbance wave number δ_r as a function of its frequency σ measured in the experiment and computed on the basis of linear stability theory. Again, a good agreement between the theory and the experiment is noted. The differences between the theoretical and experimental values increase for higher frequencies, similarly as in the case of growth rates discussed above.

Results discussed above demonstrate that the characteristics of the travelling wave disturbances measured in the experimental apparatus used in the present work agree with the predictions based on the linear stability theory. We are now in position to investigate changes in the disturbance evolution induced by the wall corrugation.

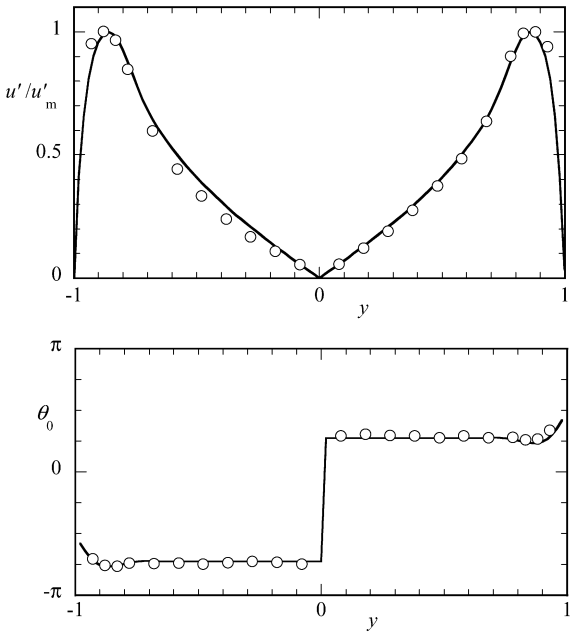

Fig. 6. The amplitude $u'(y)$ and the phase $\theta_0(y)$ distributions of the streamwise velocity fluctuation $u_3(x, y, t)$ excited at the frequency $\sigma = 0.30$ at the flow Reynolds number $Re = 5000$ in a channel with smooth walls. Circles – experiment (measured at $x - x_0 = 53.3$), solid curves – linear stability theory.

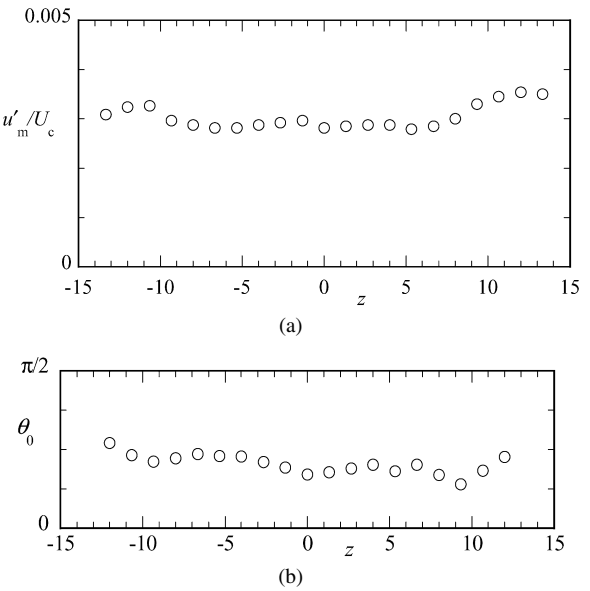

Fig. 7. Spanwise distributions of the maximum rms value u'_m of the amplitude u' and the phase θ_0 (measured at $x - x_0 = 53.3$, $y = -0.85$) of the streamwise velocity fluctuation $u_3(x, y, t)$ excited at the frequency $\sigma = 0.30$ at the flow Reynolds number $Re = 5000$ in the channel with smooth walls.

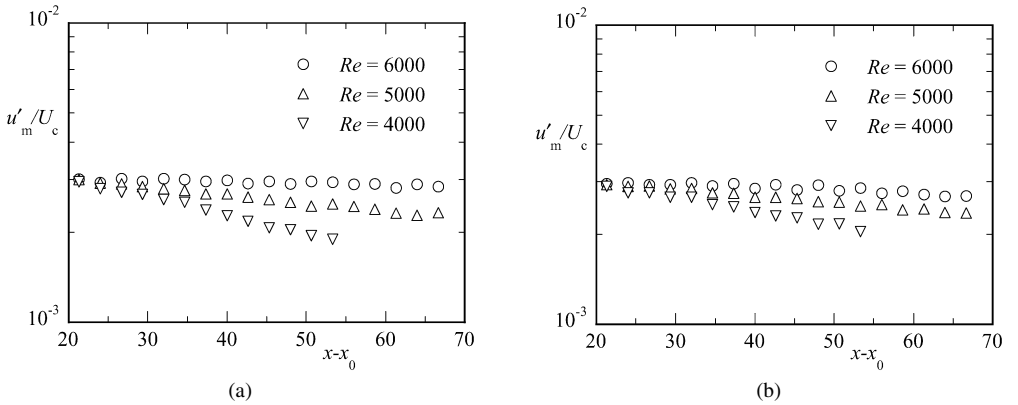

Fig. 8. Development of disturbances excited at the frequencies (a) $\sigma = 0.27$ and (b) $\sigma = 0.30$ at the flow Reynolds numbers $Re = 4000$, 5000 and 6000 in the channel with smooth walls.

3.4. Basic flow in a channel with one wavy wall

The top section of the channel closed to the channel exit was replaced with a wavy wall model, as illustrated in Fig. 2. Wall whose shape is given as $y_w = 2S\sin(\alpha x)$ with the wave number $\alpha = 1.02$ (wavelength 46.2 mm) and the amplitude $2S = 0.04$ (0.3 mm) has been selected for the experiment. This particular wave number matches the wave number of the critical disturbances in the case of smooth wall. The model had streamwise length of 415.8 mm (nine wavelengths) and was produced using CNC machining. The transition from the flat to the sinusoidal-shape surface was smoothed out to avoid appearance of a sharp convex corner. In the experiment, the wavy model was placed at the upper wall in such a way that the corrugation would begin at a distance of 260 mm from the disturbance generator ($x - x_0 = 34.7$, where x_0 denotes location of the disturbance generator). The model was placed in such a way that the

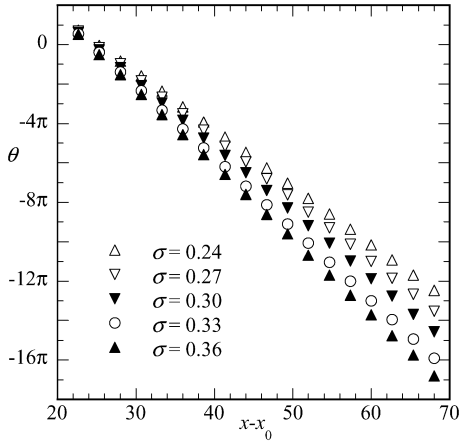

Fig. 9. Streamwise variation of the disturbance phase θ measured at $y = -0.7$ for $\sigma = 0.24$, 0.27, 0.30, 0.33 and 0.36 at $Re = 5000$ in the channel with smooth walls.

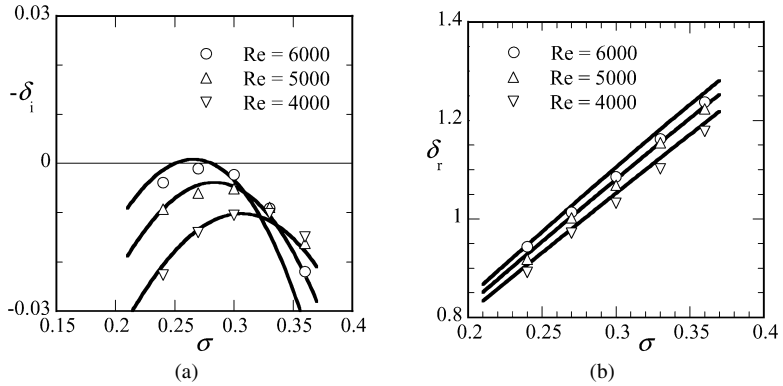

Fig. 10. Comparison of (a) the spatial growth rates δ_i and (b) the wave numbers δ_r between the linear theory and the experiment in the case of channel with smooth walls. Solid curves illustrate theoretical results.

mean location of the wavy wall overlapped with the location of the smooth wall, i.e., the mean height of the channel remained unchanged.

Placement of the wavy wall increases the overall resistance to the flow, though only slightly. For meaningful comparisons with the flow in a smooth channel, the mass flow rates for both cases must be matched. The equality of the flow rate was assured by adjusting the fan in the case of tunnel with the wavy wall. The wavy wall terminates at $x = 785$ ($14.5h$ upstream from the channel exit) so that the flow enters the smooth channel again near the exit (for $x = 785-800$). The flow at the exit thus returns to its original state with parabolic velocity distribution, and the equality of the flow rate was easily attained by adjusting the centerline velocity at the channel exit to the same value as that found in the case of smooth channel. It is also noted that the introduction of disturbances has not changed the mass flow rate, at least for the present linear stability experiment. The centreline velocity measured at the channel exit was used for defining the Reynolds number, similarly as in the case of smooth channel.

Fig. 11 displays results of measurements of the streamwise velocity component for $Re = 5000$ together with the theoretical results based on the solution $u_2(x, y)$ discussed in Section 2.1. It can be seen that the experimental apparatus closely reproduces the form of the flow predicted by the theory. The influence of the wall corrugation is only limited to the near wall region $y > 0.8$. The shape of the streamlines suggests appearance of a weak centrifugal effect that may affect stability properties of the flow. The velocity profiles across the channel become slightly inflectional near the wall over half the wavelength of the corrugation, as shown in Fig. 12. Such modulation of near-wall flow can also affect the flow stability. Finally, the reader may note bending of the vortex sheet due to the presence of the corrugation that may lead to an interesting vortex dynamics and may contribute to changes in the stability properties.

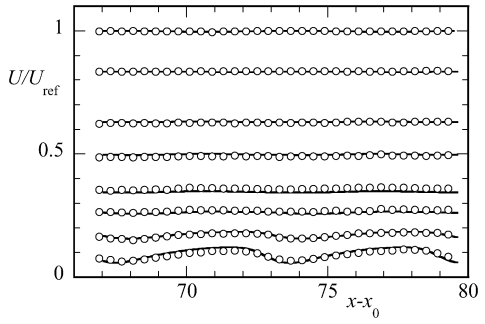

Fig. 11. Streamwise distributions of the streamwise velocity component in the upper half of the channel (adjacent to the corrugated wall) at $Re = 5000$ for the sinusoidal corrugation with the amplitude $S = 0.02$ and the wave number $\alpha = 1.02$. The distributions were measured at $y = 0$, 0.4, 0.6, 0.7, 0.8, 0.85, 0.9, 0.94 (from top to bottom). The crests of the sinusoidal corrugation (correspond to the narrowest channel openings) are located at $x - x_0 = 67.3$ and 73.5. Solid curves represent the theoretical result, $u_2(x, y)$ (Eq. (2.1)). U_{ref} is the maximum velocity measured at the first crest.

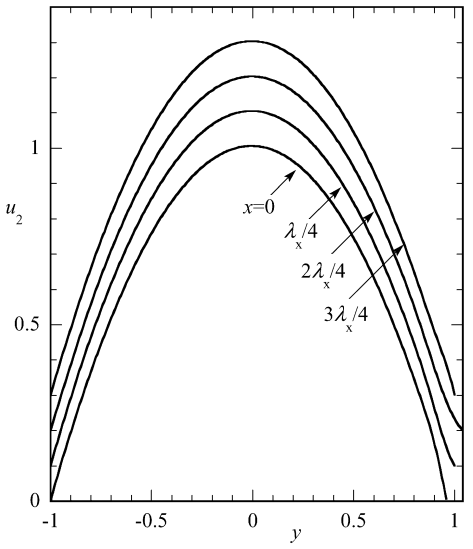

Fig. 12. Normal-to-the-wall distributions of the streamwise velocity component $u_2(x, y)$ at $x = 0$, $\lambda_x/4$, $\lambda_x/2$, $3\lambda_x/4$, where $\lambda_x = 2\pi/\alpha$ is the wavelength of the corrugation, for the flow Reynolds number $Re = 5000$ and the sinusoidal corrugation with the amplitude $S = 0.02$ and the wave number $\alpha = 1.02$. Curves corresponding to $x = \lambda_x/4$, $\lambda_x/2$, $3\lambda_x/4$ have been moved by 0.1, 0.2, 0.3 in the u_2 direction, respectively.

All these effects come into play simultaneously and could either re-enforce or cancel each other. The cumulative effect will be discussed in the next section.

3.5. Linear stability of the flow in a channel with wavy wall

The streamwise disturbance velocity component can be written as (see Eq. (2.13))

$$u_3(x, y, t) = \mathrm{e}^{\mathrm{i}(\delta x - \sigma t)}\hat{u}(x, y) + CC = \mathrm{e}^{\mathrm{i}(\delta x - \sigma t)} \sum_{m=-\infty}^{m=+\infty} u^{(m)}(y)\, \mathrm{e}^{\mathrm{i}m\alpha x} + CC$$

$$= \mathrm{e}^{-\delta_{\mathrm{i}} x} \sum_{m=0}^{m=+\infty} \left\{ \left[u^{(m)}(y)\, \mathrm{e}^{\mathrm{i}[(\delta_{\mathrm{r}} + m\alpha)x - \sigma t]} + CC \right] + \left[u^{(-m)}(y)\, \mathrm{e}^{\mathrm{i}[(\delta_r - m\alpha)x - \sigma t]} + CC \right] \right\} \tag{3.4}$$

where $\hat{u}(x, y)$denotes disturbance amplitude modulated due to the presence of the corrugation. The "primary" wave excited by the periodic forcing of frequency σ has the wave number δ_{r} and the amplitude $u^{(0)}(y)$. Wall corrugation modulates this wave. Modulation has several components that can be divided into two groups, with the first group based on differences between the wave and the corrugation wave numbers and the second one based on the sums. The modulation wave numbers and the amplitudes in the former case are $\delta_{\mathrm{r}} - m\alpha$, $u^{(m)}(y)$, $m = 1, \ldots, \infty$, respectively, and the latter case are $\delta_{\mathrm{r}} + m\alpha$, $u^{(-m)}(y)$, $m = 1, \ldots, \infty$, respectively. The spatial disturbance modulation has to be accounted for in the experiment in order to reliably measure the growth rates.

The magnitude of the streamwise disturbance amplitude modulation is directly related to the amplitude of the wall waviness. Fig. 12 illustrates distribution and magnitude of the eigenfunctions obtained for the experimental conditions of $Re = 5000$, $\alpha = 1.02$, $\sigma = 0.27$, $\delta = (1.0159, -0.008528)$. It can be seen that the eigenfunctions $u^{(m)}$, $m > 1$ and $m < -1$, are negligible for practical purposes. The form of the disturbance that we need to be concerned with in the experiment is therefore

$$u_3(x, y, t) = \mathrm{e}^{-\delta_{\mathrm{i}} x} \left\{ \left[u^{(0)}(y)\, \mathrm{e}^{\mathrm{i}(\delta_{\mathrm{r}} x - \sigma t)} + CC \right] + \left[u^{(1)}(y)\, \mathrm{e}^{\mathrm{i}[(\delta_{\mathrm{r}} + \alpha)x - \sigma t]} + CC \right] \right.$$
$$\left. + \left[u^{(-1)}(y)\, \mathrm{e}^{\mathrm{i}[(\delta_{\mathrm{r}} - \alpha)x - \sigma t]} + CC \right] \right\}. \tag{3.5}$$

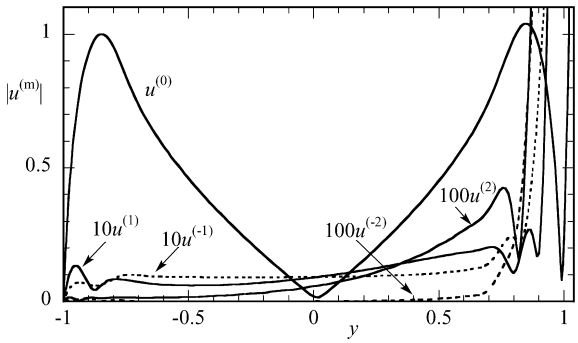

Fig. 13. Distributions of the amplitude of the eigenfunctions $|u^{(m)}(y)|$, $m = -2, -1, 0, 1, 2$, (see Eq. (3.3)) determined for the flow Reynolds number $Re = 5000$, the disturbance frequency $\sigma = 0.27$, the disturbance wave number $\delta_r = 1.0159$ and the disturbance amplification rate $\delta_i = -0.008528$ in a channel with the wavy wall of amplitude $S = 0.02$ and the wave number $\alpha = 1.02$ and normalized with condition $\max_{-1<y<0} |u^{(0)}(y)| = 1$.

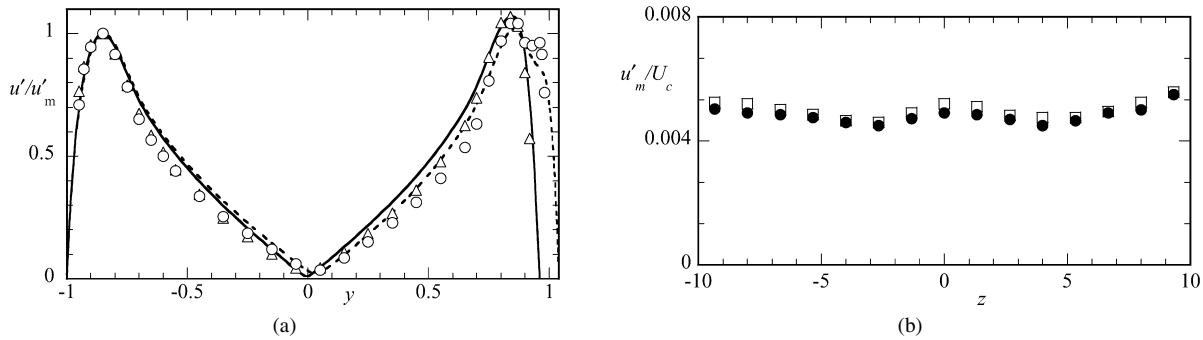

Fig. 14. The r.m.s. amplitudes u' of the streamwise disturbance velocity u_3 in a channel with the wavy wall of amplitude $S = 0.02$ and the wave number $\alpha = 1.02$. The forcing frequency $\sigma = 0.27$. (a) y-distributions of u' measured at mid-span ($z = 0$) at two x-positions corresponding to the crest (△, $x - x_0 = 67.3$) and the trough (○, $x - x_0 = 70.4$) of the corrugation. Solid curves illustrate theoretical results (Eq. (3.3)). The distributions are scaled with the maximum of u' (denoted by u'_m) at the lower half of the channel (adjacent to the smooth wall) at each x-location. (b) z-distributions of u'_m measured at upper half of the channel (□) and lower half (●) at $x - x_0 = 70.4$.

When $\alpha \cong \delta_r$, modulation has one component with the wave number nearly equal to $2\delta_r$ (it corresponds to the first superharmonic of the waviness) and second with a very small wave number $|\delta_r - \alpha| \ll 1$ that produces very long wavelength modulation that is sometimes referred to in the acoustics as the "beating" frequency. Since in the experiment we are interested in the disturbance and corrugation wave numbers close to each other, the long wavelength "beating" modulation could pose significant problem, as the length of the experimental apparatus is finite.

In order to make comparisons with the experiment it is convenient to express the disturbance quantity analogously to Eq. (3.2) as

$$u_3(x, y, t) = \hat{u}_3(x, y)\, e^{-\delta_i x} \cos\big[\delta_r x - \sigma t - \theta_3(x, y)\big]. \tag{3.6}$$

The eigenvalue $\delta_r + i\delta_i$ and the eigenfunction $\hat{u}(x, y)$ were calculated from Eqs. (2.14), (2.15) for a specified frequency σ. The experiment involved measurements of the amplification δ_i, the wave number δ_r and the amplitude $\hat{u}_3(x, y)$ for the fixed frequency σ. The reader may note that $u'(x, y)$ has a simple x-periodicity dictated by the corrugation wave number α. Results displayed in Fig. 13 demonstrate that the x-modulation of $\hat{u}_3(x, y)$ is limited to a region near the wavy wall. This modification is at most of the order of 1% of the primary component $u^{(0)}$ in the channel half adjacent to the smooth wall. This fact is better illustrated in Fig. 14(a) that displays y-distributions of the amplitudes $u'(x, y)$ measured at two locations ($x = 67.3$ and 70.4) corresponding to the crest and trough of the corrugation, respectively, as well as the corresponding theoretical results for u_3. Good agreement between both data sets demonstrates that the disturbances are little affected by the finite distance between the measurement's zone and the beginning of the waviness. We note that these results also demonstrate that the hot wire placed in the lower half (flat-plate region) of the channel would pick up signal that is very similar to that found in the case of smooth channel

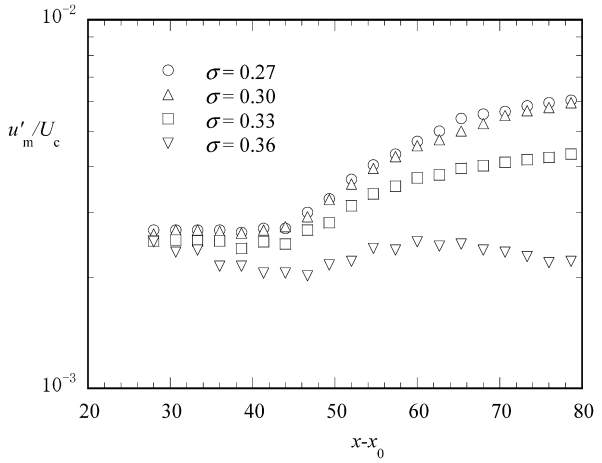

Fig. 15. Development of disturbances excited at frequencies $\sigma = 0.27$, 0.30, 0.33 and 0.36 in a channel with the wavy wall with the amplitude $S = 0.02$ and the wave number $\alpha = 1.02$ at the flow Reynolds number $Re = 5000$. u'_m was measured in the lower channel half (adjacent to the smooth wall).

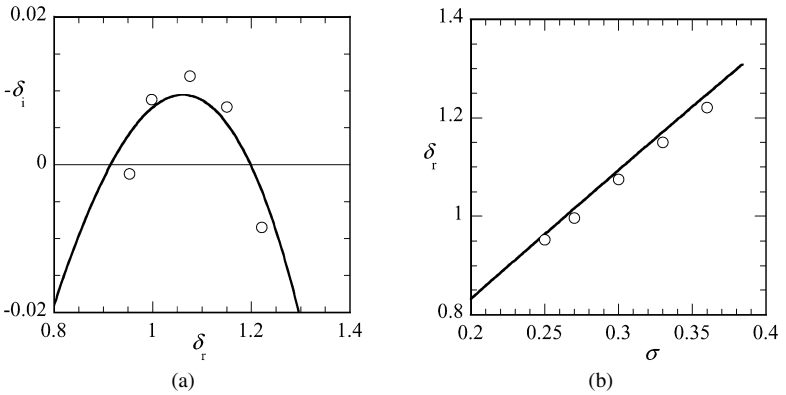

Fig. 16. Comparison of (a) the spatial growth rate δ_i and (b) the wave number δ_r between the theory and the experiment for flow with the Reynolds number $Re = 5000$ in a channel with wavy wall with the amplitude $S = 0.02$ and the wave number $\alpha = 1.02$. Open circles – experiment, solid curve – theory.

and that this signal would be very little affected by the modulation due to the wall waviness. The two-dimensionality of the amplitude distributions is shown in Fig. 14(b) which displays z-distributions of u'_m the maximum of u') measured at the lower and upper halves of the channel. Spanwise variations of the disturbance amplitude are less than 10% over $-10 < z < 10$, similar to the case of smooth channel (i.e., channel without the wall corrugation). Besides, the z-distributions in both the upper half and lower channel halves are quite similar to each other. These facts strongly suggest that the centrifugal effect due to the waviness of upper wall is very weak.

The above discussion shows that the measurements of the spatial amplification can be carried out using the same strategy as in the case of smooth walls as long as the hot wire is properly placed in the lower channel half (the half adjacent to the smooth wall).

Fig. 15 illustrates streamwise development of disturbances excited at frequencies $\sigma = 0.27$, 0.30, 0.33 and 0.36 for $Re = 5000$. The maximum u'_m of $u'(x, y)$ at each x was measured in the lower channel half. The wavy model begins in this figure at $x - x_0 = 34.7$, where x_0 denotes location of the disturbance generator (location of the downstream slot). It can be seen that the approaching disturbances decay over the smooth wall, as expected for such flow conditions, but begin to grow after entering the corrugated section. A constant growth trend emerges from the "spatial transient" at a distance of approximately four corrugation wavelengths downstream from the beginning of the corrugation. The growth rates were obtained on the basis of data taken in the "constant trend" zone by the least square method and are compared with the theoretical results in Fig. 16(a). The comparisons show good agreement with the theory, in

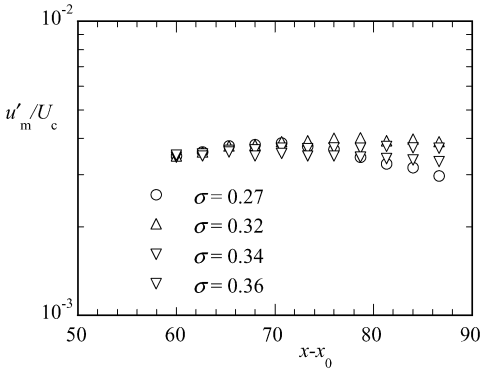

Fig. 17. Development of disturbances excited at frequencies $\sigma = 0.27$, 0.32, 0.34 and 0.36 in a channel with the wavy wall with the amplitude $S = 0.02$ and the wave number $\alpha = 1.02$ at the flow Reynolds number $Re = 4000$. u'_{m} was measured in the lower channel half (adjacent to the smooth wall).

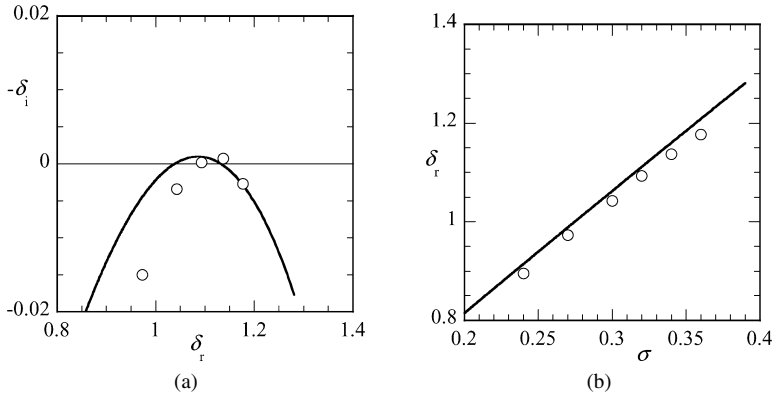

Fig. 18. Comparison of (a) the spatial growth rate δ_{i} and (b) the wave number δ_{r} between the theory and the experiment for flow with the Reynolds number $Re = 4000$ in a channel with wavy wall with the amplitude $S = 0.02$ and the wave number $\alpha = 1.02$. Open circles – experiment, solid curve – theory.

spite of the existence of the "beating" modulation that has wavelength of the order of the length of the model. Results displayed in Figs. 15 and 16(a) demonstrate that the "spatial transient" is fairly short and disturbances attain their terminal growth rate within a few corrugation wavelengths. Good agreement was also obtained for the disturbance wave number, as shown in Fig. 16(b) which displays comparison of the computed and measured disturbance wave numbers.

One point in Fig. 16(a), corresponding to $\delta_{\mathrm{r}} \cong \alpha = 1.02$, deserves a special attention as such disturbance (with $\sigma = 0.27$) is not subject to the "beating" modulation and measurements of its growth rate are, in principle, more accurate. The available results demonstrate that the difference between the theoretical and measured growth rates for this particular disturbance is similar to that observed in the case of other disturbances.

One of the objectives of the experiment is the verification of the existence of the critical Reynolds number. Fig. 17 illustrates the streamwise development of disturbances excited at frequencies $\sigma = 0.27$, 0.32, 0.34 and 0.36 at $Re = 4000$. The spatial transient region terminates around $x - x_0 = 65$ for all the cases and the disturbances exhibit constant growth rate downstream from there. Fig. 18 illustrates the measured growth rates and the wave numbers. It can be seen that the disturbance with the maximum growth rate at this Reynolds number has a wave number $\delta_{\mathrm{r}} \cong 1.1$ and the growth rate nearly zero. The reader may recall that the theory predicted the critical Reynolds number Re_{cr} to be 3900 and the corresponding critical wave number to be $\delta_{\mathrm{r,cr}} = 1.09$ (see Section 2).

4. Conclusions

Experiments designed to verify theory describing the linear stability of flow in a channel with wavy wall [1] have been carried out. The wavy wall model provides a convenient reference point for the analysis of the effects of arbitrary

surface corrugations on the stability of shear layers. Geometry of such corrugations can be expressed using Fourier series [22] and wavy wall represents a leading term in such series. The present experiment has been focused on the two-dimensional travelling wave instability.

In the experiment, disturbances of fixed frequency had been introduced using a loudspeaker system and their evolution in the downstream direction had been measured. One of the channel walls has been modified by introduction of the wavy wall model with the amplitude $2S = 0.04$ and the wave number $\alpha = 1.02$. The spatial growth rates, the disturbance wave numbers and the distribution of disturbance amplitude measured over such wall agree with the predictions based on the linear stability theory. In particular, existence of the critical Reynolds number has been confirmed experimentally. It has been confirmed that the critical Reynolds is reduced by 30% due to the presence of wall corrugation considered in this study.

Acknowledgements

This work was in part supported by the Grant-in-Aid for Scientific Research C (13650963) from the Japan Society for the Promotion of Science. The second author would like to acknowledge support obtained through the Japanese Society for the Promotion of Science and the NSERC of Canada. The SHARCNET of Canada provided the computing resources. The authors would like to thank dr. S. Krol for carrying out some of the required computations and Mr. Y. Maeda for his help in carrying out the experiment.

References

[1] J.M. Floryan, Two-dimensional instability of flow in a rough channel, Phys. Fluids 17 (2005) 044101 (also: Rept. ESFD-1/2003, Dept. of Mechanical and Materials Engineering, The University of Western Ontario, London, Ontario, Canada, 2003).
[2] G. Hagen, Über den Einfluss der Temperatur auf die Bewegung des Wasser in Röhren, Math. Abh. Akad. Wiss. Berlin (1854), pp. 17–98.
[3] H. Darcy, Recherches expérimentales relatives au mouvement de l'eau dans les tuyaux, Paris, Mallet-Bachelier, 1857, p. 268.
[4] O. Reynolds, An experimental investigation of the circumstances which determine whether the motion of water shall be direct or sinuous, and of the wall of resistance in parallel channels, Philos. Trans. Roy. Soc. London 174 (1883) 935–982.
[5] H. Schlichting, Boundary Layer Theory, seventh ed., McGraw-Hill, New York, 1979.
[6] J. Jimenez, Turbulent flows over rough walls, Annu. Rev. Fluid Mech. 36 (2004) 173–196.
[7] J. Nikuradse, Strömungsgesetze in Rauhen Röhren, VDI-Forschungscheft #361 (1993) (also NACA TM 1292 (1950)).
[8] C.F. Colebrook, Turbulent flow in pipes, with particular reference to the transition region between smooth and rough pipes, J. Inst. Civ. Engrg. 11 (1939) 133–156.
[9] L.F. Moody, Friction factors for pipe flow, Trans. ASME 66 (1944) 671–684.
[10] P. Bradshaw, A note on "critical roughness" and "transitional roughness", Phys. Fluids 12 (2000) 1611–1614.
[11] D.R. Waigh, R.J. Kind, Improved aerodynamic characterization of regular three-dimensional roughness, AIAA J. 36 (1998) 1117–1119.
[12] P.S. Klebanoff, K.D. Tidstrom, Mechanism by which a two-dimensional roughness element induces boundary layer transition, Phys. Fluids 15 (1972) 1172–1188.
[13] J.A. Masad, V. Iyer, Transition prediction and control in subsonic flow over a hump, Phys. Fluids 6 (1994) 313–327.
[14] M.V. Morkovin, On roughness-induced transition: facts, views and speculations, in: M.Y. Hussaini, R.G. Voigt (Eds.), Instability and Transition, in: ICASE/NASA LARC Series, vol. 1, Springer, 1990, pp. 281–295.
[15] J.M. Floryan, On the Görtler instability of boundary layers, Progr. Aerospace Sci. 28 (1991) 235–271.
[16] T.C. Corke, A. Bar Sever, M.V. Morkovin, Experiments on transition enhancements by distributed roughness, Phys. Fluids 29 (1986) 3199–3213.
[17] K. Sing, J.L. Lumley, Effect of roughness on the velocity profile of a laminar boundary layer, Appl. Sci. Res. 24 (1972) 168–186.
[18] M. Lessen, S.T. Gangwani, Effect of small amplitude wall waviness upon the stability of the laminar boundary layer, Phys. Fluids 19 (1976) 510–513.
[19] J.M. Kendall, Laminar boundary layer velocity distortion by surface roughness: Effect upon stability, AIAA 19th Aerospace Sciences Meeting, AIAA Paper 81-0195, 1981.
[20] C.L. Merkle, K.T.-S. Tzou, T. Kubota, An analytical study of the effect of surface roughness on boundary layer stability, Dynamics Technology Inc., Report DT-7606-4, 1977.
[21] E. Reshotko, Disturbances in a laminar boundary layer due to distributed surface roughness, in: T. Tatsumi (Ed.), Turbulence and Chaotic Phenomena, Proceedings of IUTAM Symposium, Elsevier, 1984, pp. 39–46.
[22] J.M. Floryan, Stability of wall-bounded shear layers in the presence of simulated distributed roughness, J. Fluid Mech. 335 (1997) 29–55 (also: Rept. ESFD-1/96, Dept. of Mechanical and Materials Engineering, The University of Western Ontario, London, Ontario, Canada, 1995).
[23] L. Brevdo, T. Bridges, Absolute and convective instabilities of spatially periodic flows, Philos. Trans. Roy. Soc. London Ser. A 354 (1996) 1027–1064.
[24] J.M. Floryan, Centrifugal instability of Couette flow over a wavy wall, Phys. Fluids 14 (2002) 312–322.
[25] J.M. Floryan, Vortex instability in a converging-diverging channel, J. Fluid Mech. 482 (2003) 17–50.

[26] P.J. Schmid, D.S. Henningson, Stability and Transition in Shear Flows, Applied Mathematical Sciences, vol. 142, Springer, 2001.
[27] E. Reshotko, A. Tumin, Investigation of the role of transient growth in roughness induced transition, in: 32nd AIAA Fluid Dynamics Conference, St. Louis, AIAA Paper 2002-2850, 2002.
[28] W.M. Orr, The stability or instability of the steady motions of a perfect liquid and a viscous liquid, Proc. Roy. Irish Acad. A 27 (1907) 9–27 and 69–138.
[29] A. Sommerfeld, Ein Beitrag zur hydrodynamishen Erklärung der turbulenten Flüssigkeitsbewegung, in: Atti del 4 Congr. Internat. dei Mat. III, Roma, 1908, pp. 116–124.
[30] M. Nishioka, S. Iida, Y. Ichikawa, An experimental investigation of the stability of plane Poiseuille flow, J. Fluid Mech. 72 (1975) 731–751.
[31] J. Szumbarski, J.M. Floryan, A direct spectral method for determination of flows over corrugated boundaries, J. Comput. Phys. 153 (1999) 378–402.
[32] R. Sadri, J.M. Floryan, Entry flow in a channel, Comput. & Fluids 31 (2002) 133–157.
[33] M. Asai, J.M. Floryan, Certain aspects of channel entrance flow, Phys. Fluids 16 (2004) 1160–1163.
[34] Th. Herbert, Modes of secondary instability in plane Poiseuille flow, in: T. Tatsumi (Ed.), Turbulence and Chaotic Phenomena in Fluids, North-Holland, Amsterdam, 1984, pp. 53–58.
[35] M. Asai, M. Nishioka, Origin of the peak-valley wave structure leading to wall turbulence, J. Fluid Mech. 208 (1989) 1–23.